Published in final edited form as:

Clin Cancer Res. 2021 May 15; 27(10): 2938–2946. doi:10.1158/1078-0432.CCR-20-4221.

The B7-H3-targeting antibody-drug conjugate m276-SL-PBD is potently effective against pediatric cancer preclinical solid tumor models

Nathan M. Kendsersky[1,2,†], **Jarrett Lindsay**[1,2,†], **E. Anders Kolb**[3], **Malcolm A. Smith**[4], **Beverly A. Teicher**[4], **Stephen W. Erickson**[5], **Eric J. Earley**[5], **Yael P. Mosse**[1], **Daniel Martinez**[6], **Jennifer Pogoriler**[2,6], **Kateryna Krytska**[1], **Khushbu Patel**[1,7], **David Groff**[1], **Matthew Tsang**[1], **Samson Ghilu**[8], **Yifei Wang**[9], **Steven Seaman**[10], **Yang Feng**[10], **Brad St. Croix**[10], **Richard Gorlick**[9], **Raushan Kurmasheva**[8], **Peter J. Houghton**[8,*], **John M. Maris**[1,2,*]

[1]Division of Oncology and Center for Childhood Cancer Research; Children's Hospital of Philadelphia; Philadelphia, PA, 19104; USA

[2]Perelman School of Medicine at the University of Pennsylvania; Philadelphia, PA, 19104

[3]A.I. duPont Hospital for Children; Wilmington, DE, 19803

[4]NCICancer Therapy Evaluation Program; Bethesda, Maryland, 20892

[5]RTI International; Research Triangle Park, NC, 27709

[6]Division of Anatomic Pathology; Children's Hospital of Philadelphia; Philadelphia, PA, 19104

[7]Department of Biomedical and Health Informatics, Children's Hospital of Philadelphia; Philadelphia, PA, 19104

[8]Greehey Children's Cancer Research Institute, University of Texas Health Science Center at San Antonio; San Antonio, TX, 78229

[9]Department of Pediatrics, Children's Cancer Hospital, The University of Texas MD Anderson Cancer Center; Houston, TX, 77030

[10]Tumor Angiogenesis Unit, Mouse Cancer Genetics Program (MCGP), NCI-Frederick, Frederick, MD, 21702

Abstract

Purpose: Patients with relapsed pediatric solid malignancies have few therapeutic options, and many of these patients die of their disease. B7-H3 is an immune checkpoint protein encoded by the *CD276* gene that is overexpressed in many pediatric cancers. Here, we investigate the activity of the B7-H3-targeting antibody-drug conjugate (ADC) m276-SL-PBD in pediatric solid malignancy patient-derived and cell line-derived xenograft (PDX and CDX) models.

[*]**Corresponding authors:** John M. Maris, Children's Hospital of Philadelphia, 3501 Civic Center Boulevard, Philadelphia, PA, 19104. Phone: 215-590-5244; maris@chop.edu; and Peter J. Houghton, 7703 Floyd Curl Drive, San Antonio, TX 78229; Phone: 210-562-9056; HoughtonP@uthscsa.edu.

[†]Nathan M. Kendersky and Jarrett Lindsay contributed equally to this article.

Conflict of Interest Disclosure: S.S., Y.F., and B.S.C. have filed patents related to the development of m276-SL-PBD.

Experimental Design: B7-H3 expression was quantified by RNA sequencing and by immunohistochemistry on pediatric PDX microarrays. We tested the safety and efficacy of m276-SL-PBD in two stages. Randomized trials of m276-SL-PBD of 0.5mg/kg on days 1, 8, and 15 compared to vehicle were performed in PDX or CDX models of Ewing sarcoma (N=3), rhabdomyosarcoma (N=4), Wilms tumors (N=2), osteosarcoma (N=5) and neuroblastoma (N=12). We then performed a single mouse trial (SMT) in 47 PDX or CDX models using a single 0.5 m/kg dose of m276-SL-PBD.

Results: The vast majority of PDX and CDX samples studied showed intense membranous B7-H3 expression (median H-score 177, SD 52). In the randomized trials, m276-SL-PBD showed a 92.3% response rate, with 61.5% of models showing a maintained complete response (MCR). These data were confirmed in the single mouse trial with an overall response rate of 91.5% and MCR rate of 64.4%. Treatment-related mortality rate was 5.5% with late weight loss observed in a subset of models dosed weekly x 3.

Conclusions: m276-SL-PBD has significant anti-tumor activity across a broad panel of pediatric solid tumor PDX models.

Keywords

B7-H3; CD276; antibody-drug conjugate; neuroblastoma; rhabdomyosarcoma; Ewing sarcoma; osteosarcoma; Wilms tumor

Introduction

Pediatric cancer mortality has declined by 65% since 1970 (1). A large proportion of this progress can be attributed to marked reduction in deaths from leukemia, which has been achieved through optimization of chemotherapy regimens (2). In contrast, there has been only modest improvement in survival probabilities for children, adolescents and young adults with many high-risk solid malignancies despite dramatic intensification of cytotoxic therapy (3), such that survivors face lifelong complications due to intensive, multimodal therapy, underscoring a critical need for development of new therapies for pediatric cancer (4–6). Novel therapeutic approaches are thus required to improve outcomes for high-risk childhood solid malignancies.

While immune checkpoint inhibitors have shown remarkable efficacy in many adult solid malignancies, there has not been a significant activity signal in clinical trials for patients with pediatric solid tumors (7,8), at least in part due to the fact that pediatric tumors generally have low mutation burdens and thus few neoantigens, and generally low expression of PD-L1 (9–11). CD19-directed chimeric antigen receptor (CAR) engineered T cell therapy has shown remarkable efficacy in B cell leukemias (12–14), but as yet few convincing durable responses in solid malignancies have been observed for CAR T cells targeting surface antigens relevant for pediatric solid tumors. Antibody-drug conjugates (ADCs) couple the specificity of antibodies with highly potent cytotoxic agents, conferring increased potency and potential for bystander killing not seen with monoclonal antibodies alone (15–18). There are currently ten FDA-approved ADCs for a variety of human cancers,

dozens in clinical development, but in children only ADCs against leukemias and lymphomas have been actively developed.

The B7-H3 protein (encoded from the *CD276* gene) is a checkpoint molecule that is highly expressed in pediatric solid tumors, with reportedly limited expression in normal tissues (19–25). Overexpression of B7-H3 is correlated with tumor progression, metastasis, and poor clinical outcome across a variety of malignancies (26,27). Monoclonal antibodies targeting B7-H3 cause limited toxicity and have demonstrated some anti-tumor activity in clinical trials (28,29). Furthermore, intrathecal delivery of ^{131}I-8H9 (omburtamab) is in late phase clinical development for neuroblastomas with brain and/or leptomeningeal metastasis, to date showing a manageable toxicity profile with tumoricidal doses (30). Recent work has concerned development of B7-H3 CAR-T cells (23,24), with one study demonstrating efficacy in Ewing sarcoma, osteosarcoma, and medulloblastoma xenografts (22). Finally, a pyrrolobenzodiazepine (PBD)-armed ADC against CD276 (m276-PBD, a precursor to m276-SL-PBD) showed antitumor activity in a variety of adult cancer preclinical models, including superiority over a MMAE-armed anti-CD276 ADC (31). While both PBD and MMAE are DNA-binding agents, the superiority of PBD is likely due to PBD functioning irrespective of the stage of the cell cycle, thereby eradicating both the tumor and the tumor vasculature. Together, these data suggest CD276 is a rational target for further ADC development. Here, we present results from the Pediatric Preclinical Testing Consortium (PPTC) investigation of m276-SL-PBD across a large and diverse panel of pediatric cancer patient-derived and cell line-derived xenograft (PDX and CDX) models.

Methods

RNA-sequencing Analysis

Patient-Derived Xenograft RNA-sequencing data was gathered from the Pediatric Pre-clinical Testing Consortium (PPTC) dataset available on cBioPortal (32). Normal tissue RNA-sequencing data was gathered from the Genome-Tissue Expression (GTEx) resource (https://gtexportal.org/home/). Patient tumor RNA-sequencing data was collected from the Treehouse Childhood Cancer Initiative (https://treehousegenomics.soe.ucsc.edu/), which included data from the Therapeutically Applicable Research to Generate Effective Treatments initiative (https://ocg.cancer.gov/programs/target). The associated data and code used to generate the figures are available in an open-access GitHub Repository at https://github.com/nathankendsersky/pptc_cd276.

Immunohistochemistry

Tissue microarrays (TMA) including human normal childhood tissues, human neuroblastoma primary tumors, and PDX arrays for the histologies studied here were constructed as previously described, with normal tissues obtained from surgical or autopsy specimens at the Children's Hospital of Philadelphia, as previously described (33–35). Staining was performed with a polyclonal B7-H3 antibody (R&D, AF1027) at a 1:1000 dilution. Aperio GENIE Classifier (Leica Biosystems) was used to annotate tumor regions and exclude stroma and necrosis. Tumor classification was reviewed and any discordant classifications were manually annotated by a pathologist (JP). For each tumor core, Aperio

Membrane V9 algorithm (Leica Biosystems) was used to quantify staining intensity and percentage of tumor cells stained. H-scores were calculated by the following formula [(1 x %cells intensity =1) + (2 x %cells intensity = 2) + (3 x %cells intensity = 3)]. Cores in which fewer than 100 cells were available for evaluation were excluded.

ADC generation

The antibody used to create the m276-SL-PBD ADC, called m276-SL, is a modified version of the fully human m276 IgG1 antibody (31) engineered to contain four mutations (S239C, L234A/L235A/P329G) in the Fc domain (36). The S239C mutation was used for site-specific maleimide-based PBD conjugation via a dipeptide (valine-alanine) linker (36) while the LALA-PG mutations were used to prevent undesirable interactions of the ADC with Fc receptors that could potentially result in off-target killing (37). Further details about the synthesis of the modified ADC will be published separately.

Preclinical Trials

CB17SC *scid*$^{-/-}$ female (5-8 weeks) mice (Taconic Farms, Germantown NY or ENVIGO, Indianapolis, IN) were used to propagate subcutaneous xenografts. All mice were maintained under barrier conditions and experiments were conducted using protocols and conditions in accordance with the Institutional Animal Care and Use Committee at The University of Texas Health San Antonio (UTHSA), M.D. Anderson Cancer Center and the Children's Hospital of Philadelphia. The number of mice per group (control and treatment) was varied as indicated, with 10, 2, or 1 animal(s). For randomized controlled trials with either 10 or 2 mice per arm, 0.5 mg/kg of m276-SL-PBD or (0.5mg/kg) of 100 μl/20g phosphate buffered saline was administered intraperitoneally (IP) weekly x 3 (days 1, 8, and 15). A dose of 0.5 mg/kg was chosen because it was the lowest effective dose discovered in Seaman et al. (2017) (31). For the single mouse trial (N=1) study (38), a single dose of 0.5 mg/kg m276-SL-PBD administered IP. Treatment was initiated when tumor volumes reached 200 mm^3, and tumor volume and Event-Free Survival (EFS) were monitored as previously reported (29).

Statistical Methods

A tumor *event* was defined as a quadrupling of tumor volume from the day of treatment initiation, where tumor volume was estimated from caliper measurements as $(4/3) \times \pi \times ((length + width) / 4)^3$. The exact time-to-event was estimated by interpolating between the measurements directly preceding and following the event, assuming log-linear growth. Differences in event-free survival (EFS) between experimental groups of $N > 2$ were evaluated using the Gehan-Wilcoxon test, and differences in minimum relative tumor volume (RTV; ratio of current tumor volume to volume at treatment initiation) were evaluated using the Wilcoxon rank sum test.

Area Over the Curve (AOC) is the area above the RTV growth curve but below the event threshold of RTV = 4. It was calculated for each mouse using the trapezoid rule and was then divided by 4; a day of complete tumor remission, therefore, adds exactly 1 to the AOC. The AOC is correlated with time-to-event, but also captures the maximum extent and durability of tumor remission. It is a continuous, composite measure of tumor response over

the course of the experiment and is therefore well-suited for genomic analyses of association between tumor response and specific mutations.

The objective response categories are progressive disease (PD, which is subdivided among treated mice into PD without and with growth delay, PD1 and PD2 respectively), stable disease (SD), partial response (PR), complete response (CR; no measurable tumor mass for 1 recording), and maintained complete response (MCR; no measurable tumor mass for at least 3 consecutive weekly recordings) as previously described (39). Response rate is defined as the percentage of mice with PR or better. Mice experiencing a possibly treatment-related death (i.e., drug toxicity), mice with failed engraftment, and mice which unexpectedly die for reasons unrelated to treatment are excluded from statistical analyses of time-to-event, minimum tumor volume, and objective response.

For experiments of groups of $N = 2$ mice per group, we did not perform any statistical tests of group differences but have reported all other summary statistics. For the single-mouse trial (SMT) we report time-to-event, AOC, minimum RTV, and the objective response measure for each PDX or CDX model tested.

Results

B7-H3 is highly expressed in high-risk pediatric solid malignancies with limited normal childhood tissue expression

CD276 mRNA was generally highly expressed in pediatric solid tumors, compared to generally low expression in a panel of 1641 normal tissues samples from 25 organs (Figure 1A). Likewise, *CD276* mRNA was highly expressed in each PDX model studied here (32). Ewing sarcoma models had the lowest median mRNA expression of *CD276* (median = 37.42 Transcripts Per Million, TPM, normalized by trimmed mean of M-values) whereas osteosarcomas (median = 165.92 TPM) and Wilms tumors (median = 142.29 TPM) showed the highest levels of mRNA expression (Figure 1B). Immunohistochemistry of three tumor TMAs showed strong staining across the tested patient-derived xenografts (Figure 2A–C). Osteosarcoma models showed the highest expression of CD276 (median H-score = 243.0). Overall, we observed a moderate correlation (R = 0.527 p = 7.13e-05) between mRNA (TPM) and protein expression (median H-Score) (Supplemental Figure 1). For the normal tissue array, the membrane algorithm was applied to assist in reproducible evaluation of the intensity of membranous staining, with pathologist review to determine which cell types were staining in any given tissue (Supplemental Figure 2). Strong staining (3+) was seen in the basal layer of the epidermis of the skin. Weak (2+) staining was present in the adrenal cortex, bladder urothelium, basal layer of the esophageal epithelium, prostatic epithelium, pancreatic islet tissue, ovarian stroma, splenic stroma, and a subset of pituitary cells. Staining of the bone marrow hematopoietic cells as well as the epithelium in the ileocecum, colon and stomach varied from negative (0) to weak (2+). Equivocal (1+) staining was present in a subset of cardiac myocytes, a subset of aortic stromal cells, a subset of gastrointestinal tract stromal cells (appendix, colon, small intestine, stomach), gallbladder epithelium, basal urothelium of the ureter, fallopian tube epithelium and subsets of cortical neurons, renal podocytes and subset of renal tubular cells, pancreatic exocrine tissue, hepatocytes, pulmonary epithelium, a subset of germinal center cells (lymph node, tonsils,

spleen), salivary gland acinar cells, and a subset of developing spermatozoa. Staining was negative in other tissues including cerebellum, mature bone, skeletal muscle, and thyroid.

m276-SL-PBD shows strong anti-tumor activity in pediatric patient-derived xenograft models

The efficacy and toxicity of m276-SL-PBD was initially evaluated in 26 pediatric PDX and CDX models in randomized controlled trial with either 10 or 2 mice per arm (Table 1, Supplemental Table 1). This was followed by a single mouse trial (SMT) using a single dose of m276-SL-PBD in 47 distinct models (33 PDX, 14 CDX) (Table 2) (40). m276-SL-PBD was generally well tolerated with a treatment-related mortality rate of 5.5% when administered in three weekly doses and 0% when administered as a single dose. In the randomized trials with three doses given weekly, late weight loss was observed in the Ewing sarcoma, rhabdomyosarcoma and Wilms tumor models, but not in the osteosarcoma and neuroblastoma models (Supplemental Figures 3–6). No significant weight loss was observed in the SMT with a single a single administered dose of m276-SL-PBD (data not shown).

In the randomized trials, m276-SL-PBD induced significantly prolonged event-free survival (EFS) in all tested mice across all models. The minimum relative tumor volume (RTV) in treated mice was significantly less than the starting mean tumor volume for all models studied with the exception of 1 of 5 osteosarcoma models (OS-9) and 1 of 12 neuroblastoma models (NB-1691) (Figure 3A, Supplemental Figures 3–7). m276-SL-PBD showed objective responses in all models excepting the NB-1691 neuroblastoma model (PD1 response) and the OS-9 osteosarcoma model (SD response) (Table 1). All Ewing, rhabdoid tumors, and Wilms models, and 4 of 5 osteosarcomas and 10 or 12 neuroblastomas showed a MCR (N=16) or CR (N=5). The overall response rate (PR or better) was 92.3% in the randomized trial (Supplemental Table 2). In the SMT, a single dose of m276-SL-PBD significantly prolonged EFS and decreased minimum RTV in models across all histologies tested (Figures 3B–C, Supplemental Figures 8–9). The overall response rate was 91.5% with 31/47 (66%) models showing a MCR (Table 2, Supplemental Table 2). The ten models studied in both trial designs showed concordant responses (KT-10, KT-11, Rh-18, Rh-30, Rh-36, SK-NEP-1, ES-1, NB-1643, OS-1). Across both the randomized trial and SMT, we observed no correlation between CD276 expression (mRNA or protein) and objective response category (Supplemental Figure 10).

Discussion

B7-H3 is an immunomodulatory cell surface protein in the B7 superfamily, which includes other well-characterized members such as PD-L1 (41). Here we confirm and extend the previous reports of high expression on the majority of high-risk pediatric solid tumors, with significant normal childhood tissue expression by IHC limited mainly to the basal layer of skin (not previously reported), and weak expression noted in a variety of different childhood tissues (Supplemental Figure 2) (20–25). Whether or not this normal tissue expression will be a liability for an ADC that requires internalization remains unknown. Additionally, B7-H3 has been shown to play a role in metastasis, and high B7-H3 expression is associated with poor outcomes across a variety of malignancies (23). However, the precise mechanisms

that lead to B7-H3 overexpression and how the protein exerts its pro-tumor function are not defined. Early studies suggested B7-H3 played a role in T cell co-stimulation (42,43). Other data points to a potential immunosuppressive, checkpoint mechanism (44,45). Future studies are required to more precisely define the role of B7-H3 in normal human development as well as pediatric cancer tumor cell-intrinsic and -extrinsic mechanisms of immune evasion.

B7-H3 has emerged as a promising immunotherapeutic target for a variety of cancers, with several immunotherapeutic platforms targeting this protein in development, including antibodies, bispecific antibodies, ADCs and CAR T cells (22–24,28–31). Because solid pediatric malignancies tend to have low mutational burden and immunologically cold microenvironments, which hinder adaptive immunotherapeutic approaches (9–11), ADCs may be ideal platforms for differentially expressed proteins in the plasma membrane.

We used the m276 antibody platform and covalently linked pyrrolobenzodiazapine (PBD) with a cleavable valine-alanine linker and a drug-antibody-ratio (DAR) of 2. The m276-SL-PBD ADC showed potent anti-tumor activity against pediatric solid xenografts at 0.5 mg/kg regardless of whether this was administered once or weekly for three weeks. Overall response rates above 90% in both the randomized and single mouse trials, with limited observed toxicity, is an encouraging signal for clinical development. Importantly, m276 binds human and mouse B7-H3 with equal affinity (31), which further supports a potential therapeutic index in pediatric patients. The weight loss in the multi-dose experiments in some of the sarcoma and Wilms models may be due to a cumulative effect of PBD, as has been previously observed in clinical trials of PBD-family agents (47), as well as the sensitivity of CB17SC *scid*$^{-/-}$ animals to DNA-damaging agents. No skin toxicity was observed in the mice treated in this study.

Our results with m276-SL-PBD confirm the utility of the SMT design as an efficient and accurate design for screening large panels of xenograft models. A retrospective analysis of 67 agents tested by the Pediatric Preclinical Testing Program (PPTP) using $N = 8$ or 10 mice per group evaluated whether a single mouse chosen at random predicted the group median objective response. Out of 2,134 total comparisons, the single mouse matched the group median response 78% of the time and fell within one response category away 95% of the time (40). More recent work analyzed 30 agents tested by the PPTC from 2015-2018 and observed exact and near match rates of 82% and 94%, respectively (46).

It is very likely that ADC payloads may need to be tailored to potentially unique cytotoxic vulnerabilities and mechanisms or drug resistance in childhood cancer. Especially in the relapse setting after dose intensive chemotherapy, many of the favored payloads in licensed ADCs like DM1 may not be ideal as they are substrates for P-glycoprotein and other drug efflux pumps. In addition, it was recently demonstrated that m276-SL-PBD confers advantages over m276-MMAE due to PBD-mediated eradication of tumor-associated vasculature in adult tumor xenograft models (31). However, ADCs with PBD-family cytotoxic agents have shown toxicity in the clinic (48), and the anti-tumor activity seen at 0.5 mg/kg must be viewed in the context of a dose and schedule that can be achieved in the clinic. It is reassuring in our study that de-escalation from 0.5 mg/kg weekly x 3 to a single 0.5 mg/kg dose had no impact on anti-tumor activity, suggesting that with an ideal target,

stable linker and brisk internalization kinetics, PBD containing ADCs directed at B7-H3 can be developed clinically. Our data support further development of B7-H3 ADCs for childhood cancers.

Supplementary Material

Refer to Web version on PubMed Central for supplementary material.

Acknowledgments

NCI U01 CA199287 (J.M.M.), NCI R35 CA220500 (J.M.M.), NCI U01 CA199221 (R.G.G.), NCI U01 CA199297 (P.J.H.), CPRIT RP160716 (P.J.H), NCI F31 CA239424 (N.M.K), NCI F31 CA254244 (J.L.), NCI U01 CA199222 (G.G.), and the Giulio D'Angio Endowed Chair (J.M.M.).

References

1. Siegel RL, Miller KD, Jemal A. Cancer statistics, 2019. CA Cancer J Clin. 2019;69:7–34. [PubMed: 30620402]
2. Hunger SP, Mullighan CG. Acute lymphoblastic leukemia in children. N. Engl. J. Med. 2015.
3. Perkins SM, Shinohara ET, DeWees T, Frangoul H. Outcome for children with metastatic solid tumors over the last four decades. PLoS One. 2014;9:8–13.
4. Diller L, Chow EJ, Gurney JG, Hudson MM, Kadin-Lottick NS, Kawashima TI, et al. Chronic disease in the Childhood Cancer Survivor Study cohort: A review of published findings. J Clin Oncol. 2009;27:2339–55. [PubMed: 19364955]
5. Oeffinger KC, Hudson MM. Long-term Complications Following Childhood and Adolescent Cancer: Foundations for Providing Risk-based Health Care for Survivors. CA Cancer J Clin. 2004;54:208–36. [PubMed: 15253918]
6. Hudson MM. Survivors of Childhood Cancer: Coming of Age. Hematol Oncol Clin North Am. 2008;22:211–31. [PubMed: 18395146]
7. Geoerger B, Zwaan CM, Marshall L V., Michon J, Bourdeaut F, Casanova M, et al. Atezolizumab for children and young adults with previously treated solid tumours, non-Hodgkin lymphoma, and Hodgkin lymphoma (iMATRIX): a multicentre phase 1–2 study. Lancet Oncol 2020;21:134–44. [PubMed: 31780255]
8. Davis KL, Fox E, Merchant MS, Reid JM, Kudgus RA, Liu X, et al. Nivolumab in children and young adults with relapsed or refractory solid tumours or lymphoma (ADVL1412): a multicentre, open-label, single-arm, phase 1–2 trial. Lancet Oncol [Internet]. Elsevier Ltd; 2020;21:541–50. Available from: 10.1016/S1470-2045(20)30023-1 [PubMed: 32192573]
9. Majzner RG, Heitzeneder S, Mackall CL. Harnessing the Immunotherapy Revolution for the Treatment of Childhood Cancers. Cancer Cell [Internet]. Elsevier Inc.; 2017;31:476–85. Available from: 10.1016/j.ccell.2017.03.002 [PubMed: 28366678]
10. Majzner RG, Simon JS, Grosso JF, Martinez D, Pawel BR, Santi M, et al. Assessment of programmed death-ligand 1 expression and tumor-associated immune cells in pediatric cancer tissues. Cancer. 2017;123:3807–15. [PubMed: 28608950]
11. Davis KL, Fox E, Reid JM, Liu X, Minard CG, Weigel B, et al. ADVL1412: Initial results of a phase I/II study of nivolumab and ipilimumab in pediatric patients with relapsed/refractory solid tumors—A COG study. J Clin Oncol. 2017;
12. Lee DW, Kochenderfer JN, Stetler-Stevenson M, Cui YK, Delbrook C, Feldman SA, et al. T cells expressing CD19 chimeric antigen receptors for acute lymphoblastic leukaemia in children and young adults: A phase 1 dose-escalation trial. Lancet [Internet]. Elsevier Ltd; 2015;385:517–28. Available from: 10.1016/S0140-6736(14)61403-3 [PubMed: 25319501]
13. Maude SL, Frey N, Shaw PA, Aplenc R, Barrett DM, Bunin NJ, et al. Chimeric antigen receptor T cells for sustained remissions in leukemia. N Engl J Med. 2014;371:1507–17. [PubMed: 25317870]

14. Gardner R, Wu D, Cherian S, Fang M, Hanafi LA, Finney O, et al. Acquisition of a CD19-negative myeloid phenotype allows immune escape of MLL-rearranged B-ALL from CD19 CAR-T-cell therapy. Blood. 2016;127:2406–10. [PubMed: 26907630]
15. de Goeij BECG Lambert JM. New developments for antibody-drug conjugate-based therapeutic approaches. Curr Opin Immunol [Internet]. Elsevier Ltd; 2016;40:14–23. Available from: 10.1016/j.coi.2016.02.008 [PubMed: 26963132]
16. Diamantis N, Banerji U. Antibody-drug conjugates - An emerging class of cancer treatment. Br. J. Cancer. 2016. page 362–7. [PubMed: 26742008]
17. Beck A, Goetsch L, Dumontet C, Corvaïa N. Strategies and challenges for the next generation of antibody-drug conjugates. Nat Rev Drug Discov [Internet]. Nature Publishing Group; 2017;16:315–37. Available from: 10.1038/nrd.2016.268 [PubMed: 28303026]
18. Kovtun Y V, Goldmacher VS. Cell killing by antibody-drug conjugates. Cancer Lett. 2007;255:232–40. [PubMed: 17553616]
19. Lee YH, Martin-Orozco N, Zheng P, Li J, Zhang P, Tan H, et al. Inhibition of the B7-H3 immune checkpoint limits tumor growth by enhancing cytotoxic lymphocyte function. Cell Res. 2017;27:1034–45. [PubMed: 28685773]
20. Wang L, Zhang Q, Chen W, Shan B, Ding Y, Zhang G, et al. B7-H3 is Overexpressed in Patients Suffering Osteosarcoma and Associated with Tumor Aggressiveness and Metastasis. PLoS One. 2013;8:e70689. [PubMed: 23940627]
21. Zhou Z, Luther N, Ibrahim GM, Hawkins C, Vibhakar R, Handler MH, et al. B7-H3, a potential therapeutic target, is expressed in diffuse intrinsic pontine glioma. J Neurooncol. 2013;111:257–64. [PubMed: 23232807]
22. Majzner RG, Theruvath JL, Nellan A, Heitzeneder S, Cui Y, Mount CW, et al. CAR T cells targeting B7-H3, a pan-cancer antigen, demonstrate potent preclinical activity against pediatric solid tumors and brain tumors. Clin Cancer Res. 2019;25:2560–74. [PubMed: 30655315]
23. Du H, Hirabayashi K, Ahn S, Kren NP, Montgomery SA, Wang X, et al. Antitumor Responses in the Absence of Toxicity in Solid Tumors by Targeting B7-H3 via Chimeric Antigen Receptor T Cells. Cancer Cell. 2019;
24. Nguyen P, Okeke E, Clay M, Haydar D, Justice J, O'Reilly C, et al. Route of 41BB/41BBL Costimulation Determines Effector Function of B7-H3-CAR.CD28ζ T Cells. Mol Ther - Oncolytics [Internet]. Elsevier Ltd.; 2020;18:202–14. Available from: 10.1016/j.omto.2020.06.018 [PubMed: 32728609]
25. Modak S, Kramer K, Gultekin SH, Guo HF, Cheung NKV. Monoclonal antibody 8H9 targets a novel cell surface antigen expressed by a wide spectrum of human solid tumors. Cancer Res. 2001;61:4048–54. [PubMed: 11358824]
26. Tekle C, Nygren MK, Chen YW, Dybsjord I, Nesland JM, Mælandsmo GM, et al. B7-H3 contributes to the metastatic capacity of melanoma cells by modulation of known metastasis-associated genes. Int J Cancer. 2012;130:2282–90. [PubMed: 21671471]
27. Ye Z, Zheng Z, Li X, Zhu Y, Zhong Z, Peng L, et al. B7-H3 Overexpression Predicts Poor Survival of Cancer Patients: A Meta-Analysis. Cell Physiol Biochem. 2016;39:1568–80. [PubMed: 27626927]
28. Loo D, Alderson RF, Chen FZ, Huang L, Zhang W, Gorlatov S, et al. Development of an Fc-enhanced anti-B7-H3 monoclonal antibody with potent antitumor activity. Clin Cancer Res. 2012;18:3834–45. [PubMed: 22615450]
29. Powderly J, Cote G, Flaherty K, Szmulewitz RZ, Ribas A, Weber J, et al. Interim results of an ongoing Phase I, dose escalation study of MGA271 (Fc-optimized humanized anti-B7-H3 monoclonal antibody) in patients with refractory B7-H3-expressing neoplasms or neoplasms whose vasculature expresses B7-H3. J Immunother Cancer. 2015;3. [PubMed: 25767716]
30. Kramer K, Kushner BH, Modak S, Pandit-Taskar N, Smith-Jones P, Zanzonico P, et al. Compartmental intrathecal radioimmunotherapy: Results for treatment for metastatic CNS neuroblastoma. J Neurooncol. 2010;97:409–18. [PubMed: 19890606]
31. Seaman S, Zhu Z, Saha S, Zhang XM, Yang MY, Hilton MB, et al. Eradication of Tumors through Simultaneous Ablation of CD276/B7-H3-Positive Tumor Cells and Tumor Vasculature. Cancer

Cell [Internet]. Elsevier Inc.; 2017;31:501–515.e8. Available from: 10.1016/j.ccell.2017.03.005 [PubMed: 28399408]

32. Rokita JL, Rathi KS, Cardenas MF, Upton KA, Jayaseelan J, Cross KL, et al. Genomic Profiling of Childhood Tumor Patient-Derived Xenograft Models to Enable Rational Clinical Trial Design. Cell Rep. 2019;29:1675–1689.e9. [PubMed: 31693904]
33. Kononen J, Bubendorf L, Kallioniemi A, Bärlund M, Schraml P, Leighton S, et al. Tissue microarrays for high-throughput molecular profiling of tumor specimens. Nat Med. 1998;4:798–844.
34. Pilla D, Bosisio FM, Marotta R, Faggi S, Forlani P, Falavigna M, et al. Tissue microarray design and construction for scientific, industrial and diagnostic use. J Pathol Inform. 2012;3. [PubMed: 22439123]
35. Bosse KR, Raman P, Zhu Z, Lane M, Martinez D, Heitzeneder S, et al. Identification of GPC2 as an Oncoprotein and Candidate Immunotherapeutic Target in High-Risk Neuroblastoma. Cancer Cell [Internet]. Elsevier; 2017 [cited 2019 Apr 1];32:295–309.e12. Available from: http://www.ncbi.nlm.nih.gov/pubmed/28898695 [PubMed: 28898695]
36. Jeffrey SC, Burke PJ, Lyon RP, Meyer DW, Sussman D, Anderson M, et al. A potent anti-CD70 antibody-drug conjugate combining a dimeric pyrrolobenzodiazepine drug with site-specific conjugation technology. Bioconjug Chem. 2013;24:1256–63. [PubMed: 23808985]
37. Lo M, Kim HS, Tong RK, Bainbridge TW, Vernes JM, Zhang Y, et al. Effector-attenuating substitutions that maintain antibody stability and reduce toxicity in mice. J Biol Chem. 2017;292:3900–8. [PubMed: 28077575]
38. Ghilu S, Li Q, Fontaine SD, Santi DV., Kurmasheva RT, Zheng S, et al. Prospective use of the single-mouse experimental design for the evaluation of PLX038A. Cancer Chemother Pharmacol. 2020;85:251–63. [PubMed: 31927611]
39. Robles AJ, Kurmasheva RT, Bandyopadhyay A, Phelps DA, Erickson SW, Lai Z, et al. Evaluation of eribulin combined with irinotecan for treatment of pediatric cancer xenografts. Clin Cancer Res. 2020;26:3012–23. [PubMed: 32184294]
40. Murphy B, Yin H, Maris JM, Kolb EA, Gorlick R, Reynolds CP, et al. Evaluation of alternative in vivo drug screening methodology: A single mouse analysis. Cancer Res. 2016;76:5798–809. [PubMed: 27496711]
41. Collins M, Ling V, Carreno BM. The B7 family of immune-regulatory ligands. Genome Biol. 2005.
42. Chapoval AI, Ni J, Lau JS, Wilcox RA, Flies DB, Liu D, et al. B7-H3: A costimulatory molecule for T cell activation and IFN-γ production. Nat Immunol. 2001;2:269–74. [PubMed: 11224528]
43. Luo L, Chapoval AI, Flies DB, Zhu G, Hirano F, Wang S, et al. B7-H3 Enhances Tumor Immunity In Vivo by Costimulating Rapid Clonal Expansion of Antigen-Specific CD8 + Cytolytic T Cells. J Immunol. 2004;173:5445–50. [PubMed: 15494491]
44. Veenstra RG, Flynn R, Kreymborg K, McDonald-Hyman C, Saha A, Taylor PA, et al. B7-H3 expression in donor T cells and host cells negatively regulates acute graft-versus-host disease lethality. Blood. 2015;125:3335–46. [PubMed: 25814530]
45. Steinberger P, Majdic O, Derdak S V., Pfistershammer K, Kirchberger S, Klauser C, et al. Molecular Characterization of Human 4Ig-B7-H3, a Member of the B7 Family with Four Ig-Like Domains. J Immunol. 2004;172:2352–9. [PubMed: 14764704]
46. Earley E, Gorlick R, Houghton PJ, Maris JM, Li X-N, Lock RB, et al. Abstract LB-321: Re-evaluating sample sizes in preclinical testing of patient-derived xenografts. 2019.
47. Hartley JA. The development of pyrrolobenzodiazepines as antitumour agents. Expert Opin Investig Drugs. 2011;20:733–44.
48. Saber H, Simpson N, Ricks TK, Leighton JK. An FDA oncology analysis of toxicities associated with PBD-containing antibody-drug conjugates. Regul Toxicol Pharmacol. 2019;107.

Translational relevance

B7-H3 (CD276) has emerged as a promising immunotherapy target in many human malignancies. Here, we evaluated the efficacy of the B7-H3-targeted antibody-drug conjugate m276-SL-PBD in a large panel of pediatric solid tumor patient- and cell-derived xenograft models. Potent anti-tumor activity was observed in the majority of models studied, supporting the clinical development of m276-SL-PBD in high-risk childhood solid malignancies.

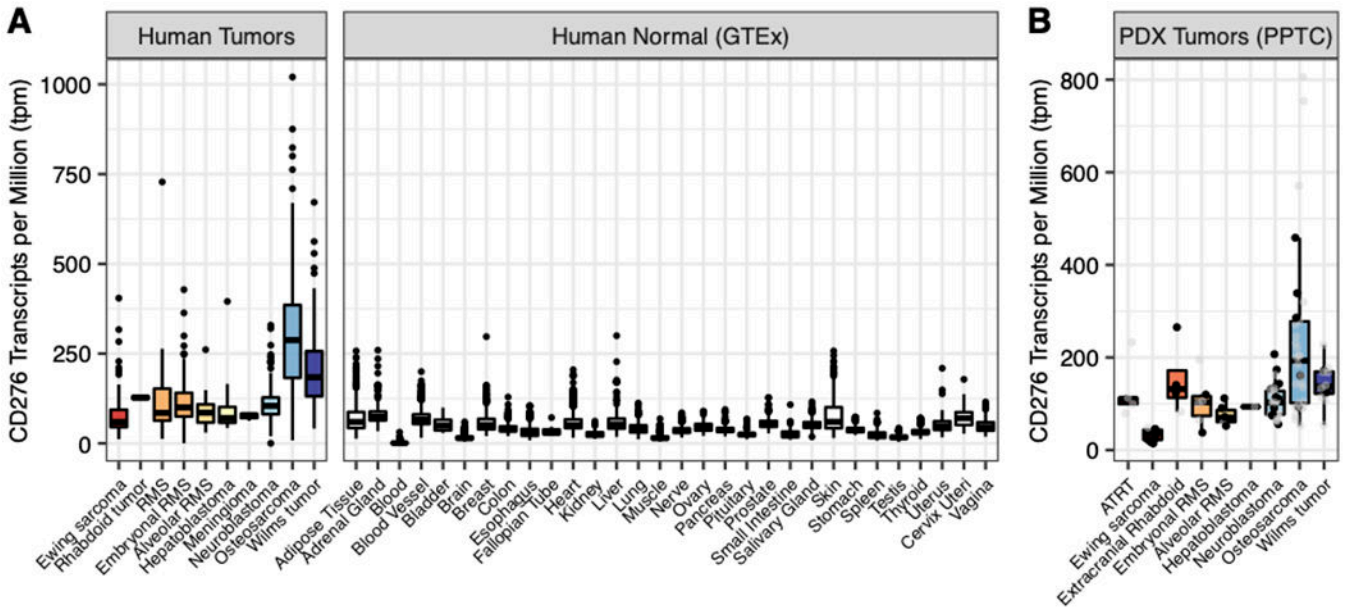

Figure 1. CD276 expression in pediatric patient-derived and cell line-derived xenograft models.

A) RNAseq expression data for CD276 in pediatric solid tumors (TARGET, Treehouse) and normal tissue samples (GTEx database). **B)** CD276 mRNA expression from PPTC RNAseq data in nine solid pediatric tumor histologies present in this study (ATRT 6; Ewing sarcoma 9; extracranial Rhabdoid 4; embryonal rhabdomyosarcoma (RMS) 6; alveolar RMS 6; hepatoblastoma 1; neuroblastoma 33; osteosarcoma 30; Wilms tumor 12). Black points in panel **B** indicate models examined in N>1 or SMT study (of 62 unique models tested, 37 had RNA-sequencing data).

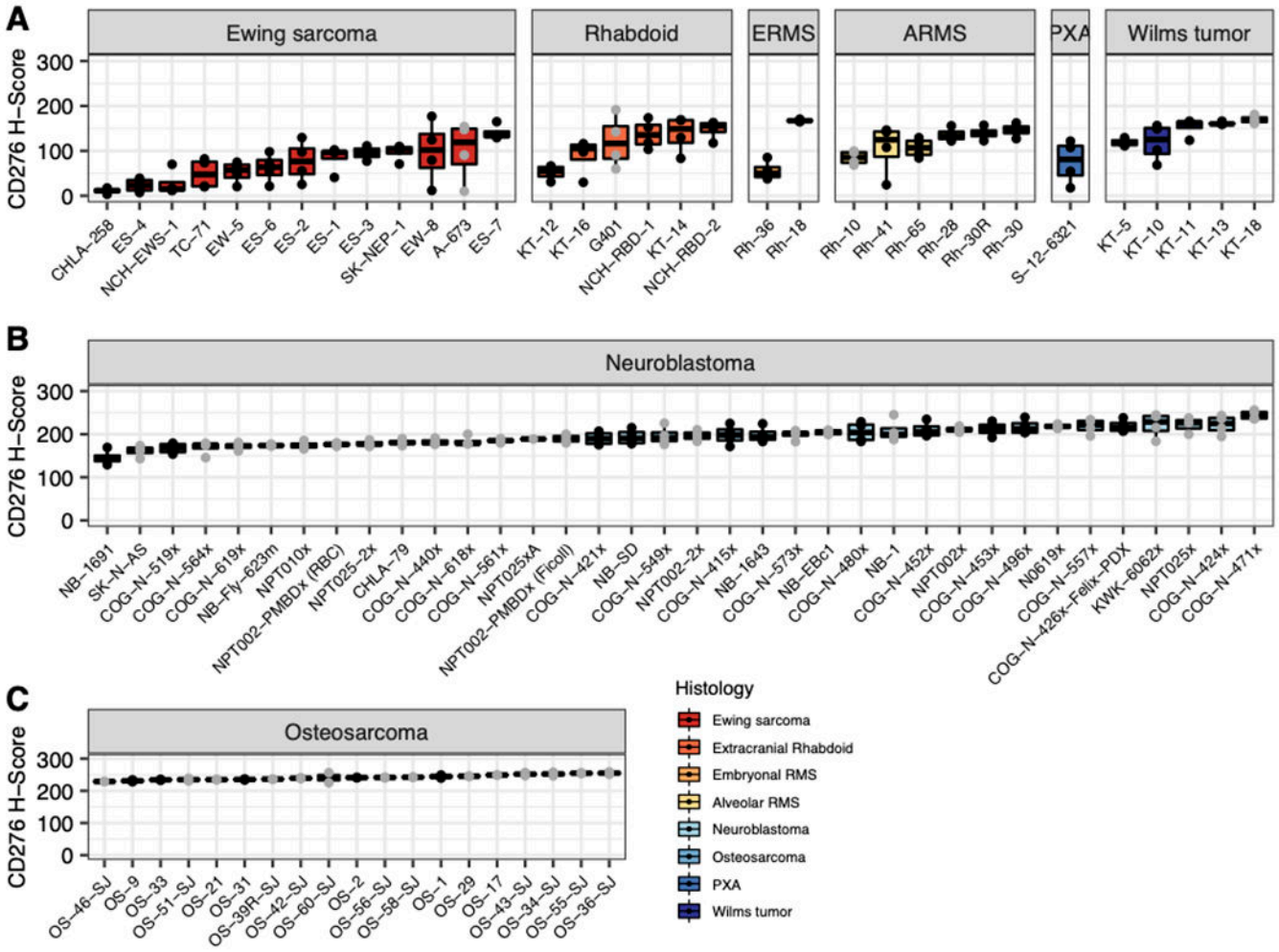

Figure 2. CD276 protein expression is elevated in pediatric patient-derived and cell line-derived xenografts.

Immunohistochemistry was performed on 3 TMAs containing mixed PDX histologies from the SMT study **(A)**, neuroblastoma models **(B)**, and osteosarcoma models (**C**). Black points indicate models examined in N>1 or SMT study.

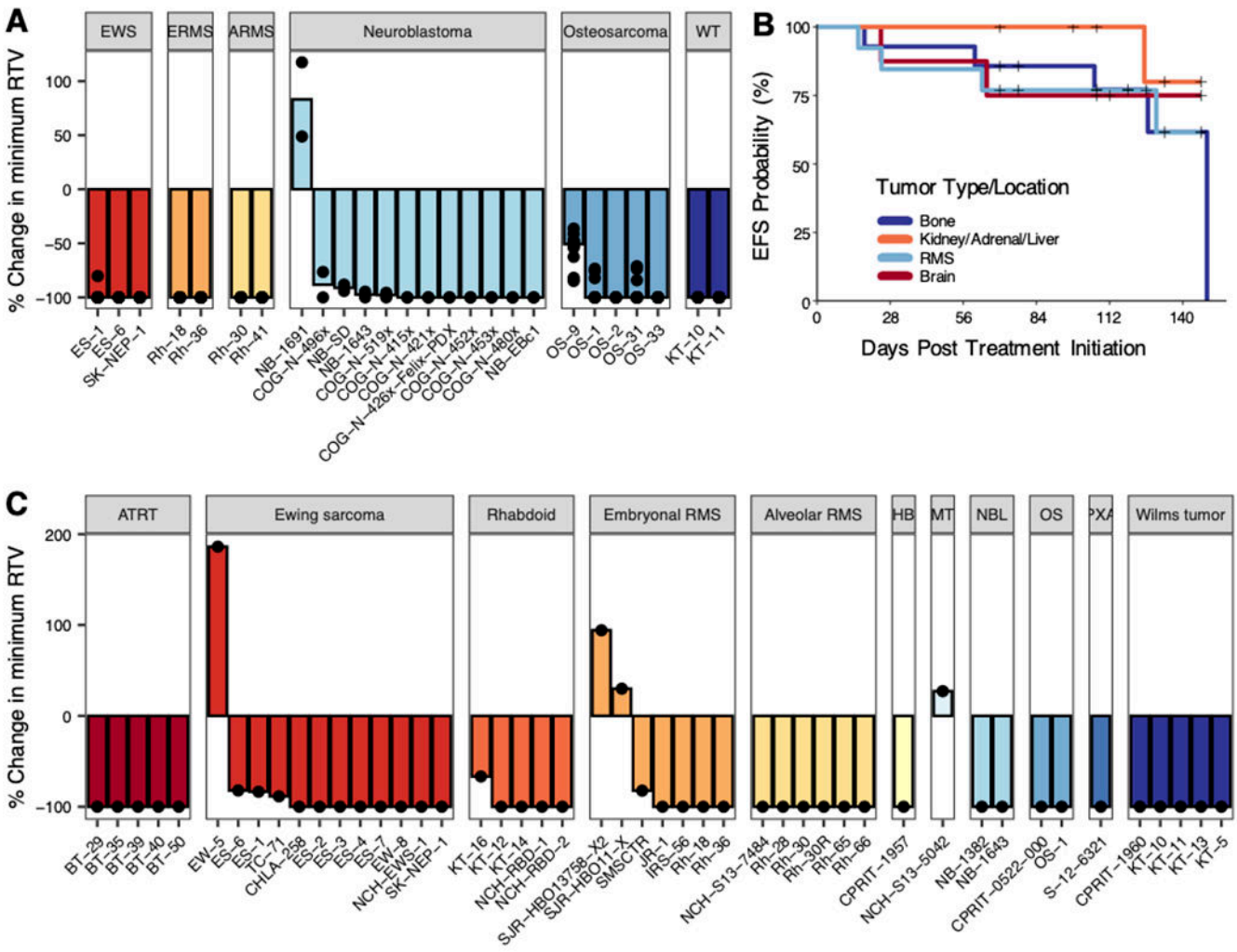

Figure 3. Tumor volume and event-free survival with m276-SL-PBD administration.

A) Waterfall plots for Ewing sarcoma (10 mice per model), rhabdomyosarcoma (10 mice per model), osteosarcoma (10 mice per model), and neuroblastoma (2 mice per model) PDX/CDXs. Bars represent median percent change in minimum relative tumor volume in treated mice. **B)** Kaplan-Meier plot of all 47 single mouse experiments (N=1) with "+" representing right-censored data. Colors represent the location of tumor origin (bone includes osteosarcoma (2 models) and Ewing sarcoma (12 models); kidney/adrenal/liver includes neuroblastoma (2 models), extracranial Rhabdoid (5 model), hepatoblastoma (1 model), and Wilms tumor (5 models); RMS includes alveolar (6 models) and embryonal RMS (7 models); brain includes ATRT (5 models), PXA (1 model), and meningioma (1 model)). **C)** Waterfall plots for models in SMT. Bars represent median percent change in minimum relative tumor volume in treated mice.

Table 1.

Activity of m276-SL-PBD across 26 Ewing sarcoma, rhabdomyosarcoma, osteosarcomas and neuroblastoma models.

KM Med = Kaplan-Meier estimate of median time-to-event, EFS T – C = difference in median time-to-event of treatment group compared to control, EFS T/C = ratio of median time-to-event of treatment group compared to control group.

Cancer Type	Model	Agent	N	KM med (days)	EFS T - C (days)	EFS T/C	p-value Gehan-Wilcoxon	minRTV mean±SD	minRTV p-value	Objective Response Measure[+]
Ewing sarcoma	ES-1[≠]	control	10	9.1				3.450±0.805		
		mCD276-SL-PBD	10	> 105	> 95.9	> 11.49	p < 0.001	0.025 ±0.070	p < 0.001	MCR
	ES-6[≠]	control	10	15.5				2.248 ±0.762		
		mCD276-SL-PBD	10	> 41	> 25.5	> 2.64	p < 0.001	0.000 ±0.000	p < 0.001	CR
	SK-NEP-1[≠]	control	10	7.6				3.521 ±1.254		
		mCD276-SL-PBD	10	> 111	> 103.4	> 14.53	p < 0.001	0.000 ±0.000	p < 0.001	MCR
Alveolar RMS (Fusion+ RMS)	Rh-30	control	10	17.2				2.033 ±0.558		
		mCD276-SL-PBD	10	> 126	> 108.8	> 7.31	p < 0.001	0.000 ±0.000	p < 0.001	MCR
	Rh-41	control	10	12.9				2.269 ±0.376		
		mCD276-SL-PBD	10	> 105	> 92.1	> 8.15	p < 0.001	0.000 ±0.000	p < 0.001	MCR
Embryonal RMS (Fusion-RMS)	Rh-18	control	10	15.0				1.873 ±0.239		
		mCD276-SL-PBD	10	> 119	> 104	> 7.91	p < 0.001	0.000 ±0.000	p < 0.001	MCR
	Rh-36	control	10	4.7				8.584 ±2.174		
		mCD276-SL-PBD	10	> 105	> 100.3	> 22.14	p < 0.001	0.000 ±0.000	p < 0.001	MCR
Wilms tumor	KT-10	control	10	13.5				2.103 ±0.372		
		mCD276-SL-PBD	10	> 98	> 84.5	> 7.26	p < 0.001	0.000 ±0.000	p < 0.001	MCR
	KT-11	control	10	13.3				2.123 ±0.385		
		mCD276-SL-PBD	10	> 105	> 91.7	> 7.9	p < 0.001	0.000 ±0.000	p < 0.001	MCR
Osteosarcoma	OS-1	control	9	32.3				1.556 ±0.244		
		mCD276-SL-PBD	10	> 76	> 43.7	> 2.36	p < 0.001	0.076 ±0.116	p < 0.001	CR
	OS-2	control	10	16.3				1.455 ±0.186		

Cancer Type	Model	Agent	N	KM med (days)	EFS T - C (days)	EFS T/C	p-value Gehan-Wilcoxon	minRTV mean±SD	minRTV p-value	Objective Response Measure[+]
		mCD276-SL-PBD	10	> 69	> 52.7	> 4.23	p < 0.001	0.000 ±0.000	p < 0.001	MCR
	OS-9	control	10	15.3				2.077 ±0.278		
		mCD276-SL-PBD	10	> 26	> 10.7	> 1.7	p < 0.001	0.442 ±0.162	p < 0.001	SD
	OS-31	control	10	20.2				1.853 ±0.291		
		mCD276-SL-PBD	10	> 62	> 41.8	> 3.07	p < 0.001	0.071 ±0.119	p < 0.001	CR
	OS-33	control	10	17.8				1.717 ±0.404		
		mCD276-SL-PBD	10	> 62	> 44.2	> 3.48	p < 0.001	0.000± 0.000	p < 0.001	MCR

Cancer Type	Model	Agent	N	KM med (days)	EFS T - C (days)	EFS T/C	minRTV mean ±SD	Objective Response Measure[+]
Neuroblastoma[◊]	COG-N-415x	control	2	6.2			2.052±0.162	
		mCD276-SL-PBD	2	46.9	40.7	7.53	0.000±0.000	MCR
	COG-N-421x	control	2	21.5			1.136±0.179	
		mCD276-SL-PBD	2	> 101	> 79.5	> 4.69	0.000±0.000	MCR
	COG-N-452x	control	2	17.8			1.069±0.062	
		mCD276-SL-PBD	2	> 102	> 84.2	> 5.73	0.000±0.000	MCR
	COG-N-453x	control	2	9.8			2.304±0.323	
		mCD276-SL-PBD	2	> 100	> 90.2	> 10.23	0.000±0.000	MCR
	COG-N-480x	control	2	12.7			1.623±0.498	
		mCD276-SL-PBD	2	> 108	> 95.3	> 8.54	0.000±0.000	MCR
	COG-N-496x	control	2	9.1			1.742±0.278	
		mCD276-SL-PBD	2	> 43	> 33.9	> 4.75	0.175±0.084	PR
	COG-N-519x	control	2	12.9			1.529±0.321	
		mCD276-SL-PBD	2	> 101	> 88.1	> 7.82	0.021±0.030	CR
	COG-N-426x-Felix-PDX	control	2	11.8			1.006±0.094	
		mCD276-SL-PBD	2	> 26	> 14.2	> 2.2	0.000±0.000	CR
	NB-1643[≠]	control	2	12.4			1.016±0.002	
		mCD276-SL-PBD	2	> 50	> 37.6	> 4.03	0.122±0.004	PR
	NB-1691[≠]	control	2	7.3			1.790±0.119	
		mCD276-SL-PBD	2	28.8	21.5	3.95	1.831±0.485	PD1

Cancer Type	Model	Agent	N	KM med (days)	EFS T - C (days)	EFS T/C	minRTV mean ±SD	Objective Response Measure[+]
	NB-Ebc1[≠]	control	2	6.8			2.888±0.698	
		mCD276-SL-PBD	2	> 102	> 95.2	> 15.02	0.000±0.000	MCR
	NB-SD[≠]	control	2	19.1			1.108±0.007	
		mCD276-SL-PBD	2	> 64	> 44.9	> 3.36	0.094±0.034	PR

◊ Note: Neuroblastoma experiments had N=2, thus p-values are not reported.

≠ cell line-derived xenograft models.

Table 2.

Activity of m276-SL-PBD (single administration) in a single-mouse testing (SMT).

Cancer Type	Model	Toxic Death	Event	Time to Event	AOC	minRTV	Objective Response Measure[+]
CNS ATRT	BT-29	0	0	> 112	> 84.2	0.000	CR
	BT-35	0	1	65.0	52.8	0.000	MCR
	BT-39	0	0	> 147	> 138.2	0.000	MCR
	BT-40	0	0	> 107	> 104.7	0.000	MCR
	BT-50	0	0	> 147	> 144.2	0.000	MCR
Ewing	CHLA-258[≠]	0	0	> 119	> 117.2	0.000	MCR
	ES-1[≠]	0	1	60.4	48.2	0.165	PR
	ES-2[≠]	0	1	149.3	133.5	0.000	CR
	ES-3[≠]	0	0	> 133	> 131.3	0.000	MCR
	ES-4[≠]	0	0	> 147	> 146.1	0.000	MCR
	ES-6[≠]	0	1	126.7	103.4	0.179	PR
	ES-7[≠]	0	0	> 107	> 98.8	0.000	MCR
	EW-5	0	1	18.1	6.2	2.862	PD1
	EW-8[≠]	0	0	> 107	> 90.0	0.000	CR
	NCH-EWS-1	0	0	> 70	> 62.9	0.000	MCR
	SK-NEP-1[≠]	0	1	106.2	81.7	0.000	CR
	TC-71[≠]	0	0	> 77	> 54.5	0.114	PR
Rhabdoid	KT-12	0	0	> 147	> 145.2	0.000	MCR
	KT-14	0	0	> 98	> 95.7	0.000	MCR
	KT-16	0	1	125.3	98.0	0.333	PR
	NCH-RBD-1	0	0	> 147	> 144.9	0.000	MCR
	NCH-RBD-2	0	0	> 70	> 69.0	0.000	MCR
ERMS (Fusion-RMS)	IRS-56	0	0	> 119	> 116.8	0.000	MCR
	JR-1[≠]	0	0	> 107	> 105.5	0.000	MCR
	Rh-18	0	1	129.9	107.2	0.000	CR
	Rh-36	0	0	> 147	> 145.6	0.000	MCR
	SJR-HBO11-X	0	1	24.7	13.0	1.299	PD1
	SJR-HBO13758-X2	0	1	15.8	6.6	1.942	PD1
	SMSCTR[≠]	0	1	63.2	45.9	0.177	PR
ARMS (Fusion+ RMS)	NCH-S13-7484	0	0	> 126	> 121.5	0.000	MCR
	Rh-28	0	0	> 77	> 75.7	0.000	MCR
	Rh-30	0	0	> 147	> 144.0	0.000	MCR
	Rh-30R	0	0	> 147	> 145.1	0.000	MCR
	Rh-65	0	0	> 133	> 131.4	0.000	MCR

Cancer Type	Model	Toxic Death	Event	Time to Event	AOC	minRTV	Objective Response Measure[+]
	Rh-66	0	0	> 70	> 66.4	0.000	MCR
Hepatoblastoma	CPRIT−1957	0	0	> 70	> 67.6	0.000	MCR
Meningioma	NCH-S13-5042	0	1	24.5	12.6	1.272	PD1
Neuroblastoma	NB-1382[≠]	0	0	> 107	> 93.3	0.000	MCR
	NB-1643[≠]	0	0	> 107	> 104.0	0.000	MCR
Osteosarcoma	CPRIT-0522-000	0	0	> 133	> 122.7	0.000	CR
	OS-1	0	0	> 107	> 102.2	0.000	MCR
PXA[*]	S-12-6321	0	0	> 147	> 145.0	0.000	MCR
Wilms	CPRIT-1960	0	0	> 70	> 66.7	0.000	CR
	KT-10	0	0	> 147	> 146.1	0.000	MCR
	KT-11	0	0	> 133	> 132.1	0.000	MCR
	KT-13	0	0	> 147	> 144.3	0.000	MCR
	KT-5	0	0	> 70	> 68.0	0.000	MCR

Note: SMT experiments had N=1, thus p-values are not reported. m276-SL-PBD was given as a single administration at 0.5 mg/kg IP.

[*] PXA, pleiomorphic xanthoastrocytoma.

[≠] cell line-derived xenograft models.